A Numerical Approach for Full-Vectorial Analysis of 3-D Guided Wave Structures With Multiple and Strong Longitudinal Discontinuities

Husain Ali Jamid and Mohd. Zahed M. Khan

***Abstract*—In this work, an accurate and efficient iterative numerical approach suitable for the analysis of 3-D guided wave structures is presented. The proposed method is fully vectorial and based on the transverse magnetic field formulation. In order to enhance the computational efficiency of the proposed method, a hybrid implementation is utilized using Padé approximants in tandem with a reduced spectrum of eigenpairs. The present formulation can account for the presence of strong and multiple longitudinal discontinuities. Convergence of this iterative approach is achieved by the use of a simple preconditioner. The accuracy and efficiency of the proposed method are demonstrated by applying it to two different guided wave structures with multiple longitudinal discontinuities.**

***Index Terms*—Waveguide discontinuities, padé approximations, 3-D waveguides, full-vectorial methods.**

I. Introduction

NUMERICAL methods are indispensable tools for the design and synthesis of guided optical structures and devices. Several propagational methods have been reported in the literature. This includes the beam propagation method (BPM) [1]–[8], the method of lines (MOL) [9]–[11], the transfer matrix method (TMM) [12], [13] and the mode matching method [14]–[17]. Purely propagational numerical methods are limited in applicability to optical structures in which the backward field may be ignored without adversely affecting the numerical results. However, a number of important guided wave structures do not satisfy this condition, which may be due to the presence of one or more sufficiently strong and abrupt longitudinal discontinuities. Obviously, propagational methods which can account for the presence of multiple longitudinal discontinuities have a wide range of applicability and can simulate optical devices with varying complexities. Various 2-D propagational methods that can account for single [1], [2], [9], [18]–[20] and multiple [3]–[8], [14]–[16] longitudinal discontinuities have been reported in the literature. Although these previously reported approaches are generally both accurate and efficient, they are limited to 2-D device simulation. The use of the more realistic 3-D model, based on the semi-vector or the full-vector field representations, is essential for accurate simulation of a number of guided optical structures. Although in principle many 2-D methods may be extended to the 3-D case, this extension usually leads to prohibitive numerical demand, which is especially true for 3-D full-vectorial models. This in turn may limit the applicability of the 3-D model to optically small devices. In the 3-D case, very little work has been reported in the literature in relation to propagational methods that account for reflection at single [21], [22] and multiple longitudinal discontinuities [10]–[12], [17]. Three dimensional propagational methods that account for *multiple* longitudinal discontinuities, under the *semi-vectorial* assumption, were reported in [12], [17], [21] and under the more realistic *full-vector* assumption were reported in [10], [11]. A variation of the MOL that utilizes a reduced spectrum of eigenpairs [10], [11] has the widest range of applicability to guided wave structures, because it can account for 3-D problems with multiple longitudinal discontinuities using a full vector formulation. Although the use of a reduced spectrum of eigenpairs enhances the efficiency of the MOL, this method may remain numerically demanding and may result in numerical instabilities in the presence of strong longitudinal discontinuities. The presence of this type of discontinuity may lead to the excitation of highly evanescent waves, which in turn leads to the requirement of a relatively large number of eigenpairs for proper satisfaction of the interface conditions and may render this method inefficient. The iterative method reported in [7] utilizes Padé approximants for the reflection and propagation operators and has been demonstrated for a 2-D corrugated waveguides with a relatively large number of longitudinal discontinuities. This iterative method is particularly interesting, because it has the potential for extension to the 3-D domain in an efficient manner. To the best of our knowledge, such extension has not been reported in the literature.

In this work, we propose to extend the method reported in [7] to three dimensions, while accounting for the full vector nature of the field, by utilizing a transverse H field formulation. To ensure rigorous satisfaction of the full vectorial boundary condition at a strong and abrupt longitudinal discontinuity, the approach reported in [22] will be utilized for this purpose. This will allow the extended method to account for multiple longitudinal discontinuities, irrespective of their strength. Two implementations of the extended method will be presented in this

Manuscript received January 13, 2008; revised April 19, 2008. Current version published December 05, 2008. This work was supported by King Fahd University of Petroleum and Minerals, Dhahran, Saudi Arabia, under Project SB070017.

H. A. Jamid is with the Electrical Engineering Department, King Fahd University of Petroleum and Minerals, Dhahran-31261, Saudi Arabia (e-mail: hajamed@kfupm.edu.sa).

M. Z. M. Khan is with the Electrical and Electronics Engineering Technology Department, Hafr Al-Batin Campus, King Fahd University of Petroleum and Minerals, Dhahran-31261, Saudi Arabia (e-mails: zahedmk@kfupm.edu.sa, zahedmk@yahoo.co.in)

Digital Object Identifier 10.1109/JQE.2008.2001938

work. The first implementation utilizes Padé approximants to account for both the reflection and propagation operators. The second implementation utilizes a hybrid approach, in which the reflection operator is calculated using Padé approximants and the propagation operator is calculated using a reduced spectrum of eigenpairs. As will be seen later, the second implementation can lead to substantial reduction in the computational time for optically large devices. Both of these implementations will be demonstrated for accuracy and efficiency. The proposed method is iterative in nature and it generally requires the use of a preconditioner for convergence of the numerical results. A simple preconditioner will be presented for this purpose.

II. Theory

A. Transverse Magnetic Field Formulation

A brief theoretical background of the transverse magnetic field formulation will be presented in this section. The reader is referred to [22] for details. Consider the 3-D wave equation

$$\frac{\partial^2 H}{\partial x^2}+\frac{\partial^2 H}{\partial y^2}+\frac{\partial^2 H}{\partial z^2}+k_0^2 n^2 H=0 \tag{1}$$

where H represents either H_x or $H_y, k_0 = 2\pi/\lambda$ is the free space wave number and n is the refractive index of the medium, which is assumed to be locally uniform. Upon discretization of (1) in the transverse dimension (x, y) using (p, q) sample points, respectively, we have

$$\frac{d^2\overline{H}}{dz^2}+\overline{Q}^2\overline{H}=\overline{0} \tag{2}$$

where the column vector $\overline{H}\equiv(\overline{H}_X\overline{H}_Y)^T$ and the column subvectors $\overline{H}_x$ and $\overline{H}_y$ contain the discretized values of H_x and H_y, respectively. The square matrix $\overline{Q}^2$ is the characteristic matrix which accounts for the spatial derivatives in the $x-y$ plane as well as coupling between the transverse magnetic field components H_x and H_y. The general solution of (2) is given by

$$\overline{H}=e^{j\overline{Q}z}\overline{A}+e^{-j\overline{Q}z}\overline{B} \tag{3}$$

where the square matrices $e^{+j\overline{Q}z}$ and $e^{-j\overline{Q}z}$ are propagational operators which account for the forward and backward fields, respectively. The discrete transverse electric field components can be expressed in terms of the transverse magnetic field components using the following matrix relationship:

$$\overline{E}=\overline{SH} \tag{4}$$

where $\overline{E}\equiv(\overline{E}_y \quad -\overline{E}_x)^T$ and the column subvectors $\overline{E}_x$ and $\overline{E}_y$ contain the discretized values of E_x and E_y, respectively. The square matrix operator:

$$\overline{S}=(j\sqrt{\mu_0/\varepsilon_0}/k_0)\overline{N}^{-2}(\overline{O}-\overline{Q}^2)(j\overline{Q})^{-1} \tag{5}$$

relates the transverse electric and magnetic field vectors. The square matrix $\overline{N}^2$ contains the discrete values of n^2 and the square matrix operator $\overline{O}$ accounts for the transverse spatial derivatives in discrete form. The square matrix $(j\overline{Q})^{-1}$ corresponds to an integration operator in the z direction.

B. Application to Multiple Longitudinal Discontinuities

Now, consider the multilayer structure shown in Fig. 1, which consists of $M+1$ abrupt longitudinal discontinuities. The semi-infinite layer $(z<0)$ is the input layer and the semi-infinite layer $(z>z_M)$ is the transmission layer. The incident transverse magnetic field vector $\bar{A}_0$ in the input layer is assumed to be known. With the exception of the transmission layer (layer $M+1$), the magnetic field within any layer contains both forward and backward components. Within the m th layer $(z_{m-1}<z<z_m)$, the transverse magnetic field can be expressed as

$$\bar{H}_m=e^{j\bar{Q}_m(z-z_{m-1})}\bar{A}_m+e^{-j\bar{Q}_m(z-z_m)}\bar{B}_m. \tag{6}$$

The continuity conditions of the transverse electric and magnetic fields at the interface $z=z_m$, are imposed using (4) and (6), which result in the following relations:

$$\overline{P}_m\overline{A}_m+\overline{B}_m=\overline{A}_{m+1}+\overline{P}_{m+1}\overline{B}_{m+1} \tag{7a}$$

$$\overline{S}_m(\overline{P}_m\overline{A}_m-\overline{B}_m)=\overline{S}_{m+1}(\overline{A}_{m+1}-\overline{P}_{m+1}\overline{B}_{m+1}). \tag{7b}$$

The matrix operator $\overline{P}_m\equiv e^{j\bar{Q}_m(z_m-z_{m-1})}=e^{j\bar{Q}_m d_m}$ where d_m correspond to the width of the m th layer. By considering all values of $m=0,1,2,\ldots,M+1$, (7) leads to a set of $2(M+1)$ equations for the unknown vectors $\bar{A}_1,\bar{A}_2,\ldots\ldots,\bar{A}_{M+1}$ and $\bar{B}_0,\bar{B}_1,\ldots\ldots,\bar{B}_M$. After some simple algebraic manipulation, these equations can be cast as a linear system of equations, which is similar, in its general form, to the one reported in [7]

$$\bar{\Gamma}\bar{\mathrm{X}}=\begin{bmatrix}\bar{\Gamma}_{11} & \bar{\Gamma}_{12}\\ \bar{\Gamma}_{21} & \bar{\Gamma}_{22}\end{bmatrix}\begin{bmatrix}\bar{\mathrm{X}}_1\\ \bar{\mathrm{X}}_2\end{bmatrix}=\begin{bmatrix}\bar{\Lambda}_1\\ \bar{\Lambda}_2\end{bmatrix}=\bar{\Lambda} \tag{8}$$

where

$$\bar{\Gamma}_{11}=\begin{bmatrix}\overline{U}_0 & \overline{Y}_1 & & & \\ & \overline{U}_1 & \overline{Y}_2 & & \\ & & \ddots & \ddots & \\ & & & \ddots & \overline{Y}_M\\ & & & & \overline{U}_M\end{bmatrix}$$

$$\bar{\Gamma}_{12}=\begin{bmatrix}\overline{0} & & & & \\ \overline{V}_1 & \ddots & & & \\ & \overline{V}_2 & \ddots & & \\ & & \ddots & \ddots & \\ & & & \overline{V}_M & \overline{0}\end{bmatrix}$$

$$\bar{\Gamma}_{21}=\begin{bmatrix}\overline{0} & \overline{Z}_1 & & & \\ & \ddots & \overline{Z}_2 & & \\ & & \ddots & \ddots & \\ & & & \ddots & \overline{Z}_M\\ & & & & \overline{0}\end{bmatrix}$$

$$\bar{\Gamma}_{22}=\begin{bmatrix}\overline{U}_0 & & & & \\ \overline{Y}_1 & \overline{U}_1 & & & \\ & \overline{Y}_2 & \ddots & & \\ & & \ddots & \ddots & \\ & & & \overline{Y}_M & \overline{U}_M\end{bmatrix}$$

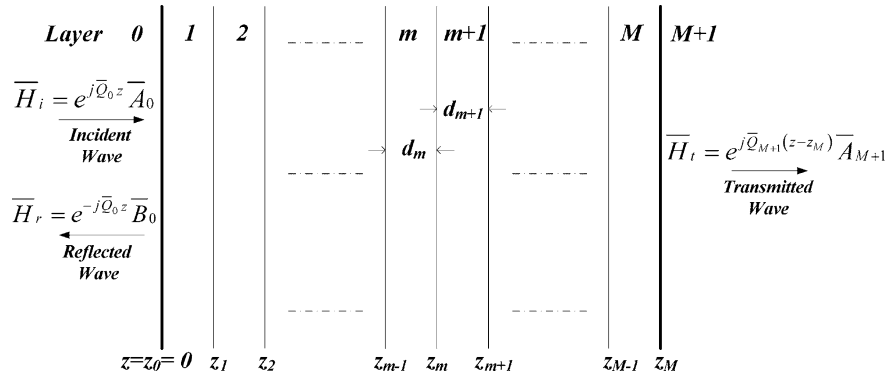

Fig. 1. Multilayer structure with abrupt longitudinal discontinuities. The incident and reflected fields exist within the left most layer and the transmitted field exists within the right most layer.

$$\bar{\mathrm{X}}_1 = [\overline{B}_0 \quad \overline{B}_1 \quad \cdots \quad \overline{B}_{M-1} \quad \overline{B}_M]^T$$
$$\bar{\mathrm{X}}_2 = [\overline{A}_1 \quad \overline{A}_2 \quad \cdots \quad \overline{A}_M \quad \overline{A}_{M+1}]^T$$
$$\bar{\Lambda}_1 = [(\overline{S}_0 - \overline{S}_1)\overline{A}_0 \quad \overline{0} \quad \cdots \quad \overline{0} \quad \overline{0}]^T$$
$$\bar{\Lambda}_2 = [(2\overline{S}_0\overline{A}_0) \quad \overline{0} \quad \cdots \quad \overline{0} \quad \overline{0}]^T$$
$$\overline{U}_m = \overline{S}_m + \overline{S}_{m+1} \quad \overline{Y}_m = -2\overline{S}_m\overline{P}_m$$
$$\overline{V}_m = -(\overline{S}_m - \overline{S}_{m+1})\overline{P}_m \quad \overline{Z}_m = (\overline{S}_{m-1} - \overline{S}_m)\overline{P}_m$$

The unknown column vector $\bar{\mathrm{X}}$ appearing in (8) contains the required reflected $\overline{B}_0$ and transmitted $\overline{A}_{M+1}$ magnetic fields as well as the magnetic field within all interior layers. The known column vector $\bar{\Lambda}$ basically contains the incident magnetic field $\bar{A}_0$. The all zero square matrices, $\overline{0}$, appearing in $\bar{\Gamma}$ and the all zero column vectors, $\overline{0}$, appearing in $\bar{\Lambda}$ are equal in size to $\overline{S}$ and $\bar{A}_0$, respectively.

In the system of linear equations represented by (8), the dimension of each of the square matrices $\overline{S}$ and $\overline{P}$ equals $2pq$ and thus the dimension of the square matrix $\bar{\Gamma}$ equals $4pq(M+1)$. For a small computational window using only 50×50 sample points in the transverse dimension and a total of only three layers in the z direction (i.e., $M = 1$), leads to a linear system with a dimension of 20 000. Obviously, this large dimension prohibits direct inversion of $\bar{\Gamma}$ and therefore solution of (8) calls for an iterative method. For this purpose, the well-known Bi-Conjugate Stabilized algorithm (Bi-CGSTAB) [19] will be used to solve (8) for the unknown vector $\bar{\mathrm{X}}$.

C. Full Padé Approach

For the present 3-D full-vector formulation, explicit calculation of the matrices $\overline{S}$ and $\overline{P}$ also becomes prohibitive, even for a small-sized computational window. In order to avoid explicit calculation of these matrices, we utilize Padé approximants with branch cut rotation, known to simultaneously account for both the propagating and evanescent waves of the spectrum [2], [8], [18], [23]. The matrix $\overline{Q}$, which is required to obtain the matrix $\overline{S}$, is found using Padé approximants of the square root operator and the matrix $\overline{P}$ is found using Padé approximants of the exponential operator. The term *Full Padé* refers to the use of Padé approximants for both $\overline{Q}$ and $\overline{P}$. The relevant expressions are respectively shown below

$$\overline{Q} = \alpha^{-1/2}\sqrt{\overline{I} + \overline{F}} = \alpha^{-1/2}\prod_{k=1}^{p_s}\frac{\overline{I} + a_k\overline{F}}{\overline{I} + b_k\overline{F}} \tag{9}$$

$$\overline{P} = e^{j\overline{Q}\Delta z} = e^{j\alpha^{-1/2}\sqrt{\overline{I}+\overline{F}}\Delta z} = \prod_{k=1}^{p_e} c_k\frac{\overline{I} + d_k\overline{F}}{\overline{I} + e_k\overline{F}}. \tag{10}$$

As shown in (9) and (10), the order of Padé approximants for $\overline{Q}$ and $\overline{P}$ are p_s and p_e, respectively. The square matrix $\overline{F} \equiv \alpha\overline{Q}^2 - \overline{I}$ where $\overline{I}$ is the identity matrix and $\alpha = \gamma e^{i\phi}$ is a branch cut rotation factor [23]. The scalar parameters a_k and b_k are Padé primes of the square root operator, are given in [5]. The scalar parameters c_k, d_k and e_k are Padé primes of the exponential operator. These parameters may be calculated using a standard method for finding Padé primes utilizing Taylor series coefficients of the exponential function. The parameter Δz represents the propagational step size. It is noteworthy to mention that $\overline{Q}$ and $\overline{P}$ appearing in (9) and (10), which are full matrices, are not calculated explicitly. Rather they are used in sparse matrix vector multiply and sparse matrix vector divide involving the submatrices of $\bar{\Lambda}$ and the corresponding subvectors of $\bar{X}$ [7].

The Full Padé formulation introduced in this section is suitable for 3-D guided wave structures exhibiting multiple and strong longitudinal discontinuities. However, its application to guided wave structures with optically wide longitudinal layer widths d_m, may lead to substantial degradation of the computational efficiency. For accurate calculation of the operator $\overline{P}$, using (10), the step size Δz must be made sufficiently small (on the order of $1.0\,\mu$m). Thus, for wide layers, repeated calculations using (10), will be necessary to account for the full layer width d_m, which may lead to poor computational efficiency. A proposed alternative approach, which overcomes this limitation, will be introduced in the next section.

D. Hybrid Approach

In (8), the matrix operator $\overline{P}$ is a *pure* propagation operator, used to account for field propagation within a specific layer. For instance, the propagation operator $\overline{P}_m$ accounts for field propagation from one end of layer m to the other end of the same layer. This operator may be implemented using a reduced spectrum of eigenpairs [10], [11], which is an alternative approach to the one expressed by (10). For a reduced set of r eigenpairs, the propagation operator may be approximated by

$$\bar{P} = e^{j\overline{Q}\Delta z} \approx \bar{T}e^{j\bar{C}\Delta z}\bar{G} \tag{11}$$

where $\bar{T} = \bar{T}_{2pq\times r}$ is a rectangular matrix containing a reduced set of r eigenvectors of the characteristic matrix $\bar{Q}^2$ and $\bar{C} = \bar{C}_{r\times r}$ is a diagonal matrix which contains the corresponding r eigenvalues. The rectangular matrix $\bar{G} = \bar{G}_{r\times 2pq}$ is the pseudo-inverse of the matrix $\bar{T}$. The matrix $\bar{G}$ can easily be calculated using the transpose of the characteristic matrix $\bar{Q}^2$ [11]. The approximate propagation operator $\bar{P}$ seen in (11) has the same dimension as the original operator, that is $\bar{P} = \bar{P}_{2pq\times 2pq}$. The accuracy of (11) depends on the number of eigenpairs used in the reduced set. One advantage of using (11) instead of (10) is that when a sufficient number of reduced eigenpairs is used, the step size Δz becomes *unrestricted* and may be made arbitrarily large. Another advantage of this equation is that, for each layer, a relatively small number of eigenpairs is required to be calculated, only once. We will later demonstrate that the use of (11) to account for the propagation operator can lead to substantial reduction in the computational time.

The matrix operator $\overline{S}$, defined by (5) is the only operator related to field reflection/transmission at a longitudinal interface between two adjacent layers (see Fig. 1). For instance, the combination of the operators $\overline{S}_m$ and $\overline{S}_{m+1}$ are the only operators that *locally* determine the reflected/transmitted field at the interface between layers m and $m+1$. It is also possible to approximate the operator $\overline{S}$ using a reduced set of eigenpairs. However, our experience shows that for sufficiently strong longitudinal discontinuities, this approximation may lead to the requirement of a very large number of eigenpairs which results in an inefficient implementation. In particular a strongly guiding structure (in the transverse direction) which simultaneously exhibits a strong longitudinal discontinuity results in the excitation of highly evanescent waves at the longitudinal interface on the low index side of the interface. In order to accurately calculate the reflected/transmitted field, highly evanescent waves must be accounted for. This leads to the requirement of a large number of eigenpairs for accurate representation of the operator $\overline{S}$. For this reason, we will use a *hybrid* approach in which the square root operator $\bar{Q}$ (and thus $\overline{S}$) is calculated using Padé approximants while the propagation operator $\bar{P}$ is calculated using a reduced set of eigenpairs.

E. Preconditioner

Solving (8) iteratively in its current form usually requires a large number of iterations and may also lead to failure of convergence of the Bi-CGSTAB algorithm. In order to reduce the number of iterations and to ensure convergence, (8) needs to be preconditioned. In this work, we propose to use a preconditioner based on first order Padé approximants. The proposed preconditioner, which is applied to (8), is

$$\bar{\delta}_m = \left(2\overline{I} + 0.5\overline{\rho}_m^{\text{avg}}\right)^{-1}\left(\overline{I} + 0.75\overline{\rho}_m^{\text{avg}}\right)\left(\overline{\kappa}_m^{\text{avg}}\right)^{-1} \qquad (12)$$

where

$$\begin{aligned}\overline{\rho}_m^{\text{avg}} &= 0.5(\overline{F}_m + \overline{F}_{m+1})\\ \overline{\kappa}_m^{\text{avg}} &= 0.5\left(\overline{N}_m^{-2}\left[\overline{O}_m - \overline{Q}_m^2\right]\right.\\ &\qquad \left.+\overline{N}_{m+1}^{-2}\left[\overline{O}_{m+1} - \overline{Q}_{m+1}^2\right]\right)\\ m &= 0, 1, \ldots, M\end{aligned}$$

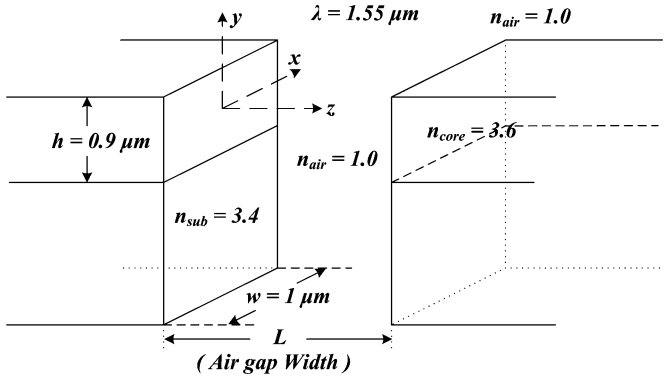

Fig. 2. Two identical channel waveguides with an air gap.

The preconditioned linear system of equations can be formulated by left multiplying the preconditioner $\bar{\delta}_m$ by *each corresponding* row of square matrices appearing in (8). For instance, $\bar{\delta}_0$ is left multiplied by the first and $(M+2)$th rows of matrices and $\bar{\delta}_1$ is left multiplied by the second and $(M+3)$th rows of matrices. The preconditioned linear system can then be solved iteratively using the Bi-CGSTAB algorithm.

III. Numerical Results

The numerical results of the full Padé and the hybrid approaches will be presented in this section and compared for accuracy and efficiency. For all calculations to be presented, the transverse computational window has been surrounded by a perfectly matched layer [24] and the input waveguide is excited by its fundamental *TE—Like* mode. Moreover, throughout this work, the magnitude and angle of the branch cut rotation factor are fixed at $\gamma = (2.25\times k_0^2)^{-1} = 2.705\times 10^{-2}$ and $\phi = -\pi/2$, respectively.

Before demonstrating the accuracy and efficiency of the proposed methods, we will first consider their convergence properties with respect to Padé order and the propagational step size Δz. For this reason, we will utilize the strongly guiding channel waveguide structure shown in Fig. 2. This structure exhibits two strong longitudinal discontinuities due to the presence of an air gap. All the relevant waveguide parameters are indicated in the same figure. Padé order associated with the reflection operator has been previously investigated for waveguides exhibiting strong longitudinal discontinuities [20], [22]. The results show that convergence of this operator is achieved at a Padé order $p_s = 3$. Therefore, in this work, this parameter is fixed at $p_s = 4$.

Next, we examine convergence of Padé approximants associated with the propagation operator, by investigating the Padé order p_e and the propagational step size Δz (see (10)). For this purpose, we calculate the modal transmissivity of the structure shown in Fig. 2, since it has been observed to be more sensitive to these two parameters than the modal reflectivity of the structure. The calculated results as a function of the step size Δz are shown in Fig. 3 for a fixed air gap width $L = 4\,\mu$m. The curves in Fig. 3(a) correspond to Padé orders $p_e = 4, 6$, and 8 at a fixed transverse mesh density of 20 points per micrometer. The modal transmissivity is seen to converge to the same value ≈ 0.015 for all the Padé orders under consideration. In addition,

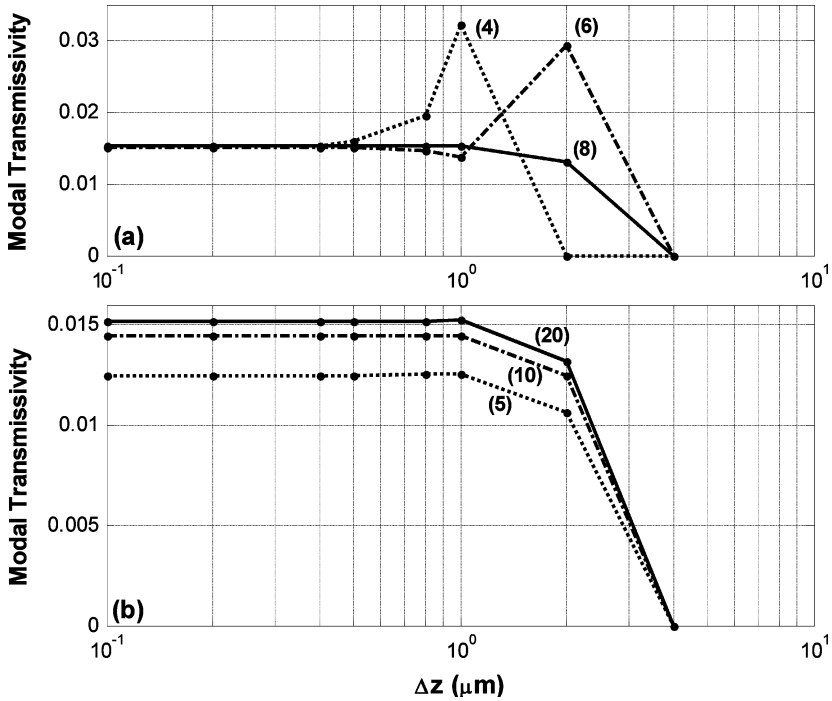

Fig. 3. Variation of the calculated modal transmissivity with the propagational step size Δz. The results correspond to the structure depicted in Fig. 2 with a 4μ m wide air gap. (a) The transverse mesh density is fixed at 20 (points/μ m), the number adjacent to each curve corresponds to the order of Padé approximant associated with the propagation operator. (b) Padé order is fixed at $p_e = 8$. The number adjacent to each curve corresponds to the transverse mesh density.

when the step size becomes very large, the calculated modal transmissivity is seen to become negligibly small. This occurs for instance when the combination $p_e = 8$ and $\Delta z = 4.0$ μm is used. For such a case, the calculated field attains very high spatial divergence, which results in negligible calculated power reaching the output waveguide. As seen in Fig. 3(a), the *edge* of convergence for Padé orders $p_e = 4$, 6 and 8 correspond *roughly* to $\Delta z = 0.4, 0.5, \text{and } 1.0$ μm, respectively. These results clearly show that lower order Padé approximants require a smaller propagational step size than higher order ones. Thus, it appears that from a computational point of view, the higher efficiency gained by utilizing lower order Padé approximants may be lost due to the lower value of the maximum allowed step size Δz. In addition, our own numerical experiments show that the use of higher order approximants give *marginally* more accurate results than lower order ones. Based on these observations and for simplicity of coding, the order of Padé approximants associated with the propagation operator will be fixed at $p_e = 8$, in *all* subsequent numerical results. The effect of the transverse mesh density on the step size Δz is illustrated in Fig. 3(b), for the selected Padé order $p_e = 8$. This figure shows the calculated modal transmissivity corresponding to mesh densities 5, 10 and 20 points per micrometer. Again, the results are seen to converge at $\Delta z \approx 1.0$ μm. The convergence edge remains at $\Delta z \approx 1.0$ μm, irrespective of the transverse mesh density. Thus, in order to operate sufficiently far from the edge of convergence, the *maximum* propagational step size, associated with Padé approximants of the propagation operator, is set to $\Delta z = 0.5$ μm, for *all* subsequent numerical results. However, it is to be stressed that the maximum step size is generally problem-dependent.

The full Padé approach will now be checked for accuracy against the well-established MOL numerical technique by applying them to the structure shown in Fig. 2, using a fixed air gap width $L = 0.5$ μ m. Fig. 4(a) shows the calculated modal reflectivity of the fundamental TE-like mode as a function of transverse mesh density. The modal reflectivity calculated using the full Padé approach is seen to converge with increasing mesh density. The MOL numerical technique used, which is based on the *full* spectrum of eigenpairs, is memory intensive and it exhausts the available computer memory beyond a mesh density of seven points per micrometer. The calculated results using the full Padé approach and the MOL are seen to be in good agreement, which establishes the accuracy of the full Padé approach. The corresponding CPU time requirements for these two techniques are shown in Fig. 4(b). The MOL is seen to require more CPU time and it exhibits a much higher rate of increase of the CPU time requirement when compared with the full Padé approach.

Fig. 5 shows the modal reflectivity of the fundamental TE-like mode as a function of the air gap width L. The transverse mesh density is fixed at 20 points per micrometer, using a transverse computational widow of size 2.6 μm $\times 3.7$ μm in the x and y directions, respectively. The calculated results using the full Padé and the hybrid approaches are shown. The full Padé results, believed to be accurate, will be used as a reference. For the hybrid approach, the calculated results correspond to 50, 100 and 200 eigenpairs. The results of the hybrid approach are seen to converge to the full Padé results as the number of eigenpairs is increased. It is interesting to note that, for the hybrid approach, when the gap width is relatively large, the number of eigenpairs required for convergence is reduced. For instance, for a

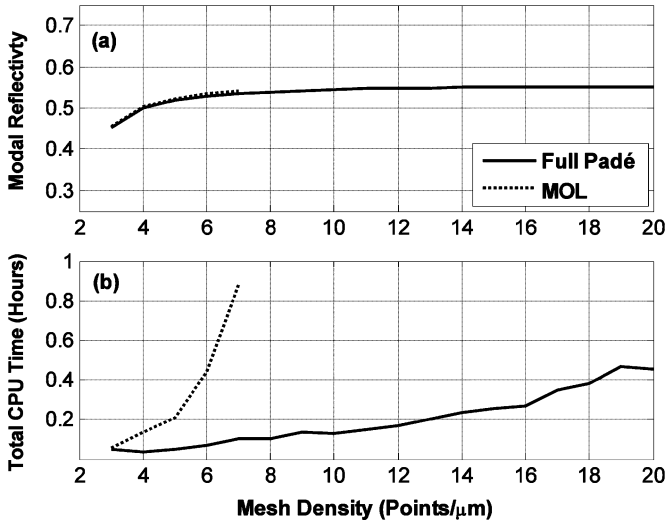

Fig. 4. (a) Variation of the fundamental TE-like modal reflectivity as a function of transverse mesh density. The results correspond to the structure depicted in Fig. 2 for a fixed air gap width of 0.5μ m. The results of the full Padé approach and the MOL numerical technique are shown. (b) The CPU runtime requirement corresponding to Fig. 4(a).

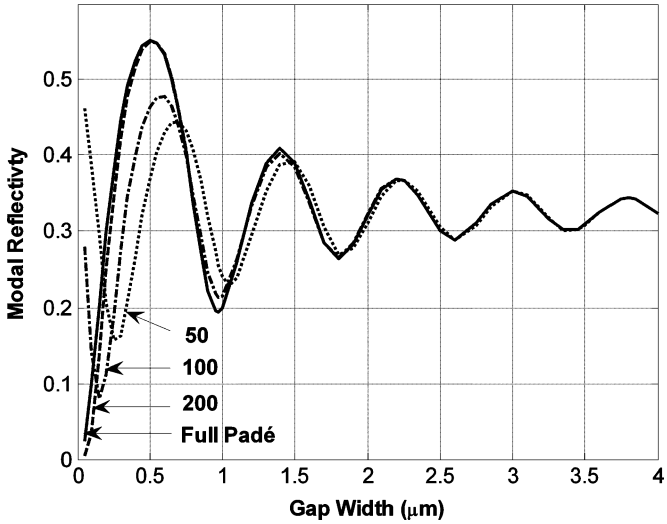

Fig. 5. Variation of the fundamental TE-like modal reflectivity as a function of air gap width. The results correspond to the structure depicted in Fig. 2. The results of the full Padé and of the hybrid approach using 50, 100, and 200 eigenpairs are shown.

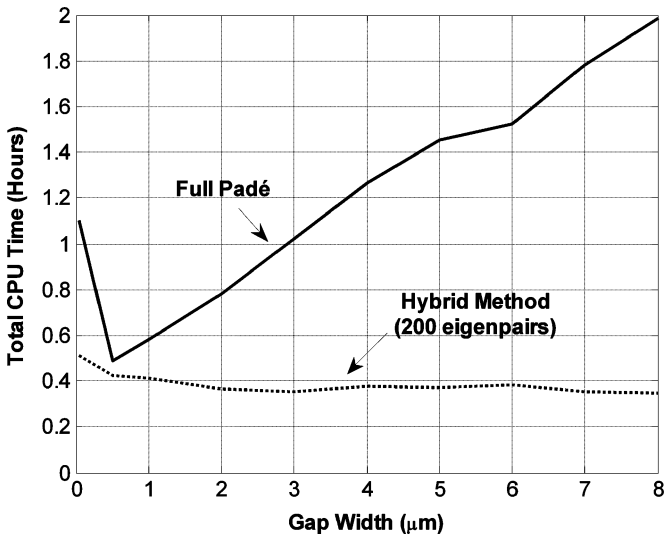

Fig. 6. CPU time requirement corresponding to Fig. 5, using an extended air gap range up to 8 μ m.

gap width larger than about 2 μm, only 50 eigenpairs are required for convergence of the hybrid method. When the number of eigenpairs is increased to 100, the calculated results begin to converge at the gap width $L \approx 1$ μm. Using 200 eigenpairs, convergent results are obtained starting at the gap width $L \approx 0.25$ μm. The reason for this behavior is easy to explain. The hybrid approach utilizes a reduced spectrum of eigenpairs to approximate the propagation operator $\bar{P}_m = \exp(j\bar{Q}_m d_m)$. When the layer width d_m becomes large, contribution of highly evanescent waves to the propagation operator $\bar{P}_m$ becomes negligible (due to their damping effect) and thus fewer number of eigenpairs are required for accurate representation of $\bar{P}_m$. On the contrary, as d_m becomes smaller, accurate representation of $\bar{P}_m$ requires increasing contribution of the evanescent waves, leading to the requirement of a larger number of eigenpairs. Another way to view this effect is by noting that when d_m is sufficiently large, the locally excited highly evanescent waves do not *link* the abrupt interfaces on either side of layer m. As a consequence, these interfaces are linked only by propagating waves and possibly also by very weakly evanescent waves. In this particular case, highly evanescent waves become important only in the determination of field reflection/transmission at these interfaces.

Fig. 6 shows the corresponding CPU time requirement of the full Padé and the hybrid approaches. In this later figure, the CPU runtime requirement has been calculated for an extended range of air gap width, up to $L = 8\mu$m. This is done to clearly illustrate the relative time requirements of each approach when the layer width becomes relatively large. For each run, the Bi-CGSTAB algorithm requires a different number of iterations to converge, which explains the non-monotonic nature of the curves shown in Fig. 6. Typical number of iterations required by the Bi-CGSTAB algorithm to converge to the results shown in Fig. 5 is roughly 20. The CPU time requirement corresponding to the full Padé approach shows a general increase with the gap width L. However, for the hybrid approach using 200 eigenpairs, the CPU time requirement remains relatively low and substantially independent of the air gap width. For a gap width $L = 8$ μm, the CPU time requirement of the hybrid approach is roughly six times less than the requirement of the full Padé method. This demonstrates that the use of the hybrid approach can lead to substantial increase in the computational efficiency.

The polarization rotator depicted in Fig. 7, [10], [11], [13] has been selected in order to demonstrate the full-vectorial capability of the current formulation. The fundamental *TE—Like* mode of the input channel waveguide, which is almost completely polarized in the horizontal direction, is used as excitation. The polarization rotation angle $\theta \equiv \tan^{-1}\sqrt{P_{\rm TM}/P_{\rm TE}}$, where $P_{\rm TE}$ and $P_{\rm TM}$ are respectively the TE and TM polarized powers. All other relevant parameters are indicated in the

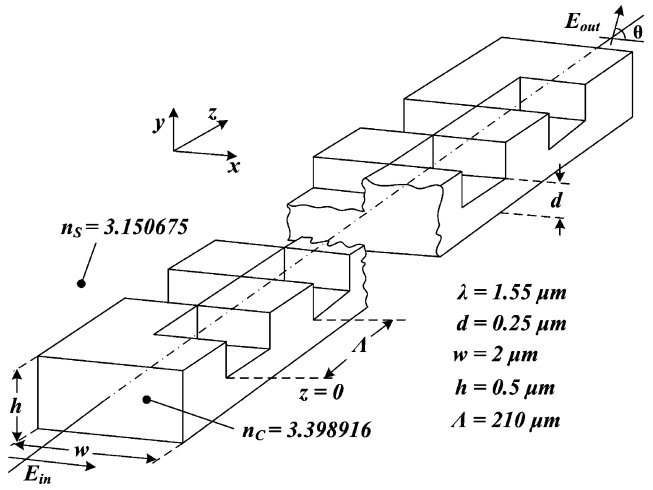

Fig. 7. Guided wave polarization rotator.

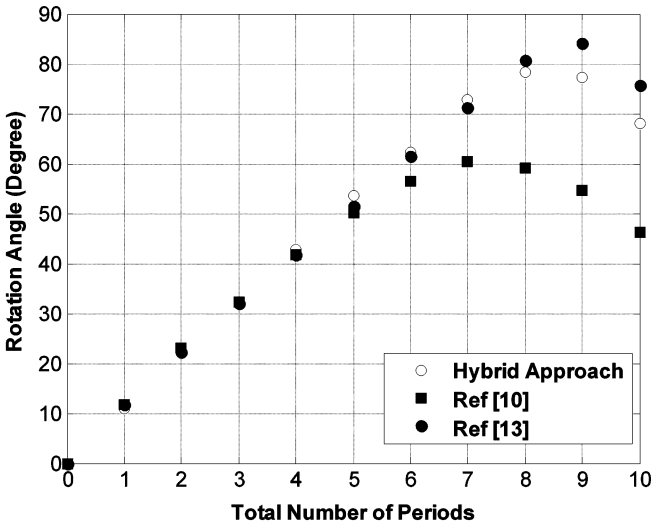

Fig. 8. Rotation angle and as a function of the total number of periods. The curves show the results of the hybrid approach and previously reported results.

figure. This periodic structure has equal longitudinal layer widths $d_m = 105\ \mu$m, corresponding to one half period of the polarization rotator. Although in principle the full Padé method is applicable for the analysis of this device, it is expected to be extremely inefficient due to the large values of d_m. For this reason we will resort to the hybrid approach for the analysis of this structure, by equating the step size and the layer width (i.e., $\Delta z = d_m$). For the polarization rotator shown in Fig. 7, we utilize a transverse computational window of size $5.0\ \mu\text{m} \times 3.5\ \mu$m in the x and y directions, respectively. In order to obtain convergent results, a transverse mesh density of 16 points per micrometers and 150 eigenpairs have been used in the hybrid approach. Fig. 8 shows the calculated rotation angle as a function the total number of periods. The calculated results using the hybrid approach are seen to be in good agreement with those reported in [10] up to 6 periods, beyond which significant difference is seen between the two results. However, our results are seen to be in good agreement with those reported in [13] up to 8 periods. A possible cause of disagreement between our results and those reported in [13] for 9 and 10 periods, may be due to the fact the calculated polarization rotation angle θ, is sensitive to small errors in the calculated TE-polarized power at large angles. In addition, the numerical approach reported in [13] ignores reflection and excitation of radiative waves at the interface, which may be another source of disagreement.

IV. Conclusion

In this paper, an iterative approach for the analysis of 3-D full-vectorial guided wave structures exhibiting multiple and strong longitudinal discontinuities has been presented. A full Padé approach and a more efficient variation using a hybrid method were presented. The hybrid method utilizes Padé approximants in tandem with a reduced set of eigenpairs. This combination utilizes the ability of Padé approximants, with branch cut rotation, to efficiently account for strong longitudinal discontinuities, and the efficiency of eigenpair decomposition to account for the propagation operator. The accuracy and efficiency of the present formulation have been demonstrated by applying it to two 3-D guided wave structures with multiple longitudinal discontinuities.

References

[1] P. Kaczmarski and P. E. Laggasse, "Bidirectional beam propagation Method," *Electron. Lett.*, vol. 24, no. 11, pp. 675–676, May 1988.
[2] H. Rao, M. J. Steel, R. Scarmozzino, and R. M. Osgood, Jr., "Complex propagators for evanescent waves in bidirectional beam propagation method," *J. Lightw. Technol.*, vol. 18, no. 8, pp. 1155–1160, Aug. 2000.
[3] H. Rao, M. J. Steel, R. Scarmozzino, and R. M. Osgood, Jr., "VCSEL design using the bidirectional beam-propagation method," *IEEE J. Quantum Electron.*, vol. 37, no. 11, pp. 1435–1440, Nov. 2001.
[4] P. L. Ho and Y. Y. Lu, "A bidirectional beam propagation method for periodic waveguides," *IEEE Photon. Technol. Lett.*, vol. 14, no. 3, pp. 325–327, Mar. 2002.
[5] P. L. Ho and Y. Y. Lu, "A stable bidirectional propagation method based on scattering operators," *IEEE Photon. Technol. Lett.*, vol. 13, no. 12, pp. 1316–1318, Dec. 2001.
[6] H. Rao, R. Scarmozzino, and R. M. Osgood, Jr., "A bidirectional beam propagation method for multiple dielectric interfaces," *IEEE Photon. Technol. Lett.*, vol. 11, no. 7, pp. 830–832, Jul. 1999.
[7] Y. Y. Lu and S. H. Wei, "A new iterative bidirectional beam propagation method," *IEEE Photon. Technol. Lett.*, vol. 14, no. 11, pp. 1533–1535, Nov. 2002.
[8] H. El-Refaei, D. Yevick, and I. Betty, "Stable and noniterative bidirectional beam propagation method," *IEEE Photon. Technol. Lett.*, vol. 12, no. 4, pp. 389–391, Apr. 2000.
[9] R. Pregla and E. Ahlers, "The method of lines for the analysis of discontinuities in optical waveguides," *Electron. Lett.*, vol. 29, no. 21, pp. 1845–1847, Oct. 1993.
[10] J. Gerdes, S. Helfert, and R. Pregla, "Three-dimensional vectorial eigenmode algorithm for nonparaxial propagation in reflecting optical waveguide structures," *Electron. Lett.*, vol. 31, no. 1, pp. 65–66, Jan. 1995.
[11] S. F. Helfert, A. Barcz, and R. Pregla, "Three-dimensional vectorial analysis of waveguide structures with the method of lines," *Opt. Quantum Electron.*, vol. 35, pp. 381–394, 2003.
[12] M. Reed, P. Sewell, T. M. Benson, and P. C. Kendall, "Efficient propagation algorithm for 3-D optical waveguides," *Proc. IEE Optoelectron.*, vol. 145, no. 1, pp. 53–58, Feb. 1998.
[13] F. J. Mustieles, E. Ballesteros, and F. Hernandez-Gil, "Multimodal analysis method for the design of passive TE/TM converters in integrated waveguides," *IEEE Photon. Technol. Lett.*, vol. 5, no. 7, pp. 809–811, Jul. 1993.
[14] G. Sztefka and H. P. Nolting, "Bidirectional eigenmode propagation for large refractive index steps," *IEEE Photon. Technol. Lett.*, vol. 5, no. 5, pp. 554–557, May 1993.
[15] O. P. Franza and W. C. Chew, "Recursive mode matching method for multiple waveguide junction modeling," *IEEE Trans. Microw. Theory Techn.*, vol. 44, no. 1, pp. 87–92, Jan. 1996.

[16] A. Theocharidis, T. Kamalakis, and T. Sphicopoulos, "Accuracy of coupled-mode theory and mode-matching method in the analysis of photonic crystal waveguide perturbations," *J. Lightw. Technol.*, vol. 25, no. 10, pp. 3193–3201, Oct. 2007.
[17] K. Jiang and W. P. Huang, "Finite-difference-based mode-matching method for 3-D waveguide structures under semivectorial approximation," *J. Lightw. Technol.*, vol. 23, no. 12, pp. 4239–4248, Dec. 2005.
[18] H. El-Refaei, I. Betty, and D. Yevick, "The application of complex padé approximants to reflection at optical waveguide facets," *IEEE Photon. Technol. Lett.*, vol. 12, no. 2, pp. 158–2000, Feb. 2000.
[19] S. H. Wei and Y. Y. Lu, "Application of Bi-CGSTAB to waveguide discontinuity problems," *IEEE Photon. Technol. Lett.*, vol. 14, no. 5, pp. 645–647, May 2002.
[20] Y. P. Chiou and H. C. Chang, "Analysis of optical waveguide discontinuities using the padé approximants," *IEEE Photon. Technol. Lett.*, vol. 9, no. 7, pp. 964–966, Jul. 1997.
[21] N. N. Feng and W. P. Huang, "Field-based numerical method for three-dimensional analysis of optical waveguide discontinuities," *IEEE J. Quantum Electron.*, vol. 39, no. 12, pp. 1661–1665, Dec. 2003.
[22] H. A. Jamid and M. Z. M. Khan, "3-D Full-vectorial analysis of strong optical waveguide discontinuities using padé approximants," *IEEE J. Quantum Electron.*, vol. 43, no. 4, pp. 343–349, Apr. 2007.
[23] D. Yevick, "The application of complex padé approximants to vector field propagation," *IEEE Photon. Technol. Lett.*, vol. 12, no. 12, pp. 1636–1638, Dec. 2000.
[24] H. A. Jamid, "Enhanced PML performance using higher order approximation," *IEEE Trans. Microw. Theory Techn.*, vol. 52, no. 4, pp. 1166–1174, Apr. 2004.

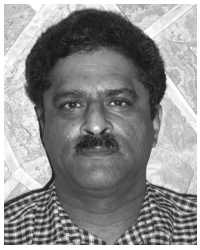

Husain A. Jamid received the B.S. and M.S. degrees in electrical engineering from Arizona State University, Tempe, Arizona, in 1981 and 1983, respectively, and the Ph.D. degree in electrical engineering from King Fahd University of Petroleum and Minerals (KFUPM), Dhahran, Saudi Arabia, in 1986.

He is currently a Professor with the Electrical Engineering Department, KFUPM. He has done research work in metal-clad as well as nonlinear optical waveguides. His current research interest is in optical device simulation and development of related numerical methods. He was the electrical engineering subject editor for the Arabian Journal for Science and Engineering from 2005 to 2007.

Dr. Jamid is three times the recipient of KFUPM Excellence in Teaching Award.

Mohd. Zahed M. Khan was born in Hyderabad, India. He received the B.E. degree in electronics and communication from Osmania University, India, in 2001, and the M.S. degree in electrical engineering from King Fahd University of Petroleum and Minerals, Dhahran, Saudi Arabia, in 2004.

Since 2004, he has been with the Electrical and Electronics Engineering Technology Department of Hafr Al-Batin Community College, King Fahd University of Petroleum and Minerals, where he currently holds the position of a Lecturer. His current area of research is the modeling and simulation of 3-D optical waveguide problems. His main area of interest includes integrated optics, digital communication and digital electronics.